# Design of a High-performance Flat Reflector Antenna Based on Conformal Transformation Optics

**Fateme Nazarzadeh**
Yazd University
**Abbas Ali Heidari** ( aheidari@yazd.ac.ir )
Yazd University

**Research Article**

**Keywords:** Reflector Antenna, dielectric, CST Studio

**Posted Date:** January 14th, 2022

**DOI:** https://doi.org/10.21203/rs.3.rs-1240274/v1

# Design of a high-performance flat reflector antenna based on conformal transformation optics

Fateme Nazarzadeh and Abbas Ali Heidari*

Department of Electrical Engineering, Yazd University, Yazd, Iran.

* Corresponding author (aheidari@yazd.ac.ir)

**Abstract**

**In this paper, we design an implementable high-performance flat reflector based on conformal transformation optics. In the proposed 2-dimensional device, the rescaling refractive index approach is applied to overcome the sub-unit refractive index issue, resulting in an all-dielectric isotropic graded-index medium that is physically implementable. Rotating the permeability profile around the antenna axis yields the 3-dimensional profile of the flat reflector construction. The dielectric with continuous refractive index profile is split into eleven layers with a constant refractive index. The proposed antenna requires only dielectric layers with the permittivity of 1.1 to 3.8, making it realizable. Simulation results show that the proposed flat reflector can operate in wide frequency bandwidth. The simulated antenna gain is about 25.27 to 29.55 dBi in the 13-30 GHz frequency range with the side-lobe level below -15 dB. Design and simulation of the proposed antenna are done using COMSOL Multiphysics, and simulation results are validated with CST Studio Suite.**

Transformation optics (TO) was proposed for the first time by Pendry in 2006 and received much attention to design the devices with unique features[1]. This mathematical method relates electromagnetic fields and materials between two spaces, namely virtual and physical, and manipulates electromagnetic waves as desired[2]. While two spaces are mathematically similar, they are related by an appropriate coordinate transformation that appears in the various constitutive parameters of medium. The main idea of TO was introduced to design an invisible cloak to hide an object from human view, but later it was utilized to design other electromagnetic devices such as cloaking[3–5], couplers[6,7], lenses[8,9], directivity enhancement in antennas, and wave transformer[10–16], polarization splitters[17–20], beam expander, and beam bends[21–23].

Despite the exciting properties of transformation optics, the materials produced by this approach are inhomogeneous and anisotropic, limiting bandwidth and complicating implementation. Two classes of transformation optics are conformal TO (CTO) and quasi-conformal TO(QCTO)[8–10,24–26]. Limiting the coordinate transformation to a conformal mapping leads to isotropic constitutive parameters for the material and a more straightforward implementation. However, QCTO does not eliminate the anisotropic nature of the environment but minimizes it. Using CTO between the virtual and physical spaces, one should find a conformal mapping between two quadrilaterals with an equal conformal module. The conformal module for a rectangle is its aspect ratio. Sometimes, it is impossible to find the same conformal module between two desired spaces, hence QCTO is used. Thus, the problem of anisotropy and magnetic medium obtained from the TO is solved using CTO/QTCO, but the inhomogeneous property of the materials are still problematic. There are various methods for implementing these

mediums with dielectric graded-index, such as dielectric drilling[27], lithography[28,29], and graded photonic crystals[12,30].

Transformation optics often lead to a sub-unit refractive index (n<1) which can be implemented by resonant metamaterials, but reduces the frequency bandwidth. There are several techniques to solve the problem of sub-unit refractive index. In usual, these values are removed or replaced with the refractive index of one (n=1), which affects the structure's performance, especially when the areas with sub-unit refractive index play a significant role in the structure's performance[12,31,32]. In the other method, all refractive index values are multiplied by a constant number, increasing the refractive index in whole structure areas. The third way is rescaling the optical path. An increasing function vs. the optical path is used in this strategy. Multiplying the derivative of an increasing function by the structure's initial refractive index yields the refractive index with optimum values. In this method, the refractive index changes, but the wavefront does not change[33].

Parabolic reflector antennas are used as high gain antennas in most communication systems. These antennas have high radiation efficiency, but are bulky and heavy due to the curved reflective surface. In certain applications, like as satellite communications, the antenna must be compact in size and volume while yet providing good gain. Furthermore, reflectarray antennas are commonly used which are flat and compact but have limited bandwidth[34]. Hence, the design of an implementable high bandwidth flat reflector antenna similar to a conventional parabolic reflector is remarkable.

Flat devices based on the transformation optics were introduced in previous researches. A discrete coordinate transformation method was investigated to design a flat antenna[31]. By choosing the proper grid in the main space, near-orthogonal meshes in transformed space can be created, resulting in a medium with low anisotropy. The same method was used to design a beam-steerable flat reflector which results from displacement between feed and reflector[32]. The bandwidth of this reflector is 13-17 GHz, and its side-lobe level is less than -7 dB. In both designs, the sub-unit refractive index values are omitted. Moreover, there is a small amount of anisotropy due to discrete coordinate transformation that affects the device's performance. A scannable flat reflector was proposed using Schwarz-Christoffel transformation that produces a conformal mapping between the virtual and physical spaces[35]. As a result, the material is entirely isotropic and does not degrade the antenna performance. However, due to the replacement of the subunit refractive index values by one, the scan angle of flat reflector is different from the desired angle.

In this paper, we present a high-performance broadband flat reflector antenna with an all-dielectric graded-index medium. We use conformal mapping to convert an ordinary parabolic reflector to a flat one. To achieve the mapping, the conformal module value in virtual and physical spaces is precisely the same. To reduce the device dispersion, the sharp edges of the virtual space are improved. Furthermore, we use the optical path rescaling method to improve the refractive indexes which are controlled by considering an appropriate increasing function. The selection of a proper scaling function consists of two steps. In the first step, the increasing function is obtained using the genetic algorithm optimization for the areas with a refractive index greater than one. The second step determines the function according to the lowest refractive index value to increase the values below one. After modifying the refractive index, the final profile of flat reflector is obtained by rotating the permittivity profile around the propagation

direction. The far-field pattern of the antenna is investigated in two simulation environments, COMSOL and CST which confirms proper performance in a wide bandwidth. Eleven layers approximate the designed permittivity profile with different values between 1.1 and 3.8. In general, the proposed device has advantages such as isotropic structure, excellent performance, broadband, low side-lobe level, small size, and physically realizable. The rest of the paper is arranged as follows: We first present the theory of transformation optics and the design process. Then, the simulation results are investigated. Finally, we end the paper with concluding remarks.

## Design Method

### Transformation Optics and CTO

The theory of transformation optics expresses a relation between two spaces: virtual space ($x$, $y$, $z$) and physical space ($x'$, $y'$, $z'$) in cartesian coordinate so that a proper coordinate transformation connects their variables. The permittivity $\varepsilon'$ and permeability $\mu'$ in physical space are obtained as

$$\varepsilon' = \frac{J\,\varepsilon J^T}{\det(J)}, \quad \mu' = \frac{J\,\mu J^T}{\det(J)} \tag{1}$$

Where $\varepsilon$ and $\mu$ are permittivity and permeability in virtual space, respectively, and $J = \partial(x', y', z')/\partial(x, y, z)$ is the Jacobian matrix. Virtual space is usually considered a vacuum with $\mu = \varepsilon = 1$, in which a beam propagates in a straight line, while the direction of beam propagation is designed arbitrarily in physical space. To simplify, consider a two-dimensional mapping between $(x, y)$ and $(x', y')$ spaces in the form of $x = u(x', y')$, $y = v(x', y')$ and $z = z'$. A conformal mapping is obtained by applying the Cauchy-Riemann equations, leading to simple constitutive parameters of the material given as[36] $\varepsilon' = \mu' = diag(1,1,(detJ)^{-1})$. Consequently, conformal mapping results in an all-dielectric material ($\mu = 1$) if the waves are limited to TE polarization (The constitutive parameters are: $\varepsilon_{zz}, \mu_{xx}, \mu_{xy}, \mu_{yx}, \mu_{yy}$ that $\mu_{xx}$=$\mu_{yy}$=1 and $\mu_{xy}$=$\mu_{yx}$=0). The refractive index of CTO transformed media can be written as

$$n = \sqrt{\varepsilon_{zz}} = \sqrt{(\det J)^{-1}} \tag{2}$$

In the following, we apply a CTO to transform a conventional parabolic reflector (with perfect electric conductor (PEC) boundary condition) into a flat one. Fig.1 shows 2-dimentional (2-D) virtual and physical spaces. Virtual space is shown in Fig.1a which consists of the reflector antenna connected to the rectangle section of ABEF to find the identical conformal module between two spaces. Two Laplace equations with Dirichlet and Neumann boundary conditions can be written as[37]:

$$\begin{gathered} u_{xx} + u_{yy} = 0\ ,\ v_{xx} + v_{yy} = 0 \\ u\big|_{AB} = -f\ ,\ u\big|_{EF} = f\ ,\ \hat{n}.(\nabla u)\big|_{up\ and\ down} = 0 \\ v\big|_{AF} = a\ ,\ v\big|_{BCDE} = b\ ,\ \hat{n}.(\nabla v)\big|_{left\ and\ right} = 0 \end{gathered} \tag{3}$$

Where $\hat{n}$ is the normal vector to the boundaries. Conformal module (M) in virtual space is given by:

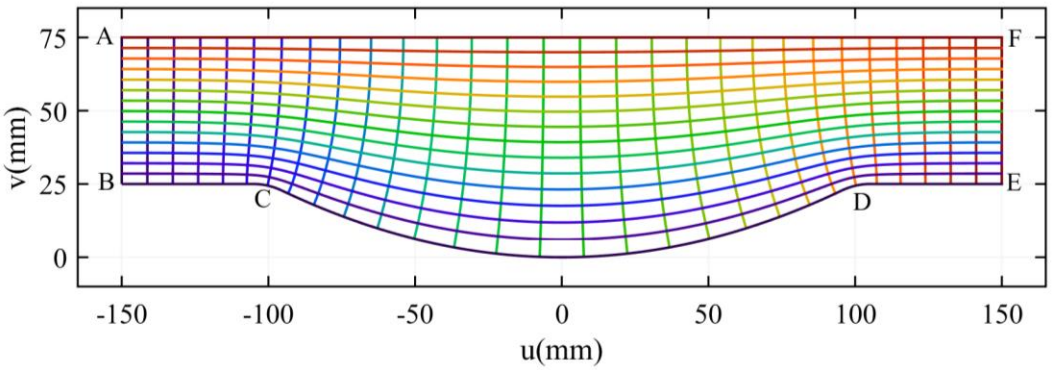


(a)

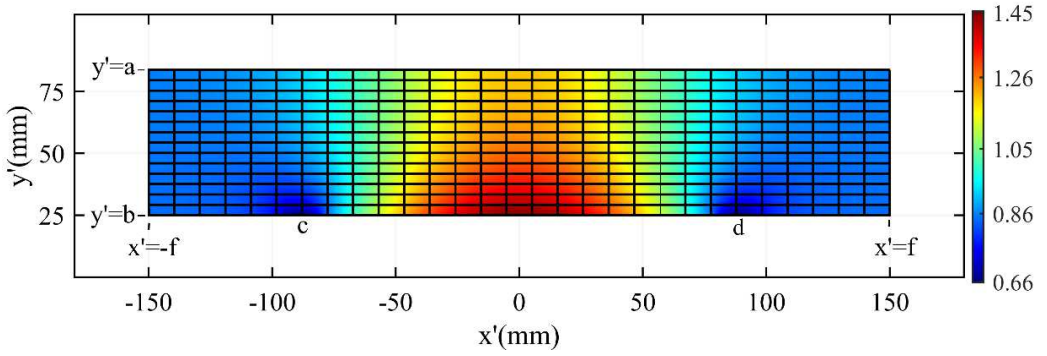


(b)

**Figure1.** The schematics of (a) virtual space with *u* and *v* contours, and (b) physical space with equivalent contours. The refractive index is also plotted.

$$\nabla^2 v = 0 \ , \ v = 0 \text{ on } BCDE \ , \ v = 1 \text{ on } AF \ , \ \frac{\partial v}{\partial n} = 0 \text{ on } AB \text{ and } FE$$

$$M = \iint_z |\nabla v|^2 dxdy = \iint_z \left[ \left( \frac{\partial v}{\partial x} \right)^2 + \left( \frac{\partial v}{\partial y} \right)^2 \right] dxdy \tag{4}$$

The design is for a parabolic reflector with diameter $d$=10$\lambda$=200$mm$ and focal length $f$=5$\lambda$=100$mm$ at the central frequency of 15 $GHz$. Therefore, we have in virtual space, $E$=$B$=7.5$\lambda$=150$mm$, $D$=$C$=100$mm$, also in physical space, $x'$=7.5$\lambda$=150$mm$, $b$=25$mm$, $a$=83.7$mm$. The points $C$ and $D$, in virtual space, are mapped to $c$=$d$=87.65$mm$ in physical space (Fig. 1).

We calculate the conformal module using PED module in COMSOL Multiphysics solver, which the result is M=5.11 for our design. The rectangular aspect ratio in physical space is accomplished with this number. Thus, we may get this ratio by altering the length or width of the physical space, but altering the rectangle width improves physical space performance. We change the junction point between the parabolic and straight lines (points $C$ and $D$ in Fig.1a) from sharp edges to smoother ones to reduce dispersion. Figure.2 shows the changed structure that the sharp edges are eliminated.

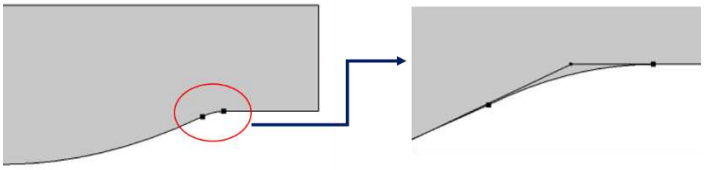

**Figure2.** Eliminating the sharp edges of the structure.

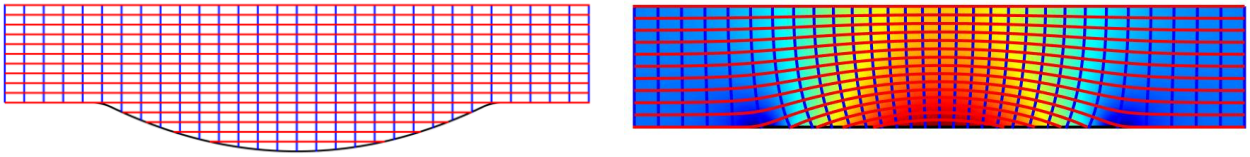

(a) (b)

**Figure 3.** The ray direction (blue lines) and phase-front (red lines). (a) in the virtual space, and (b) in the physical space.

Moreover, the distance *cd* in physical space is less than *CD* in virtual space. The refractive index is obtained from Eq. 2 in physical space and is presented in Fig.1b. As mentioned, the refractive index contains sub-unit values that in previous researches were ignored. The smallest values are related to points *C* and *D* in virtual space or equivalently *c* and *d* in physical space.

## Refractive Index Control

To adjust the refractive index and resolve the sub-unit refractive index problem, we apply the rescaling optical path method which improves the structure's performance. Assume that a plane wave propagates in virtual space from top to bottom. The vertical lines (blue lines) in Fig. 3a show the ray direction, and the horizontal lines (red lines) are the wave phase-fronts. The equivalent of these lines in physical space is shown in Fig. 3b. The optical path length is the distance that light travels in a space with a specified refractive index. The optical path length is significant because it allows us to determine the wave phase at any point. The relationship between the optical path length and the refractive index is defined as

$$u = \int_{A}^{B} n \, dl \tag{5}$$

Where $u$ and $n$ are the optical path length and the refractive index as a function of the distance along the ray from point A to point B, respectively. Moreover, we can consider the refractive index as

$$n(x, y) = \left|\nabla u\right| \tag{6}$$

We consider an increasing function such as *S(u)* called the "rescaled optical path" and assume that *S(u)* measures the optical path instead of $u$, so the refractive index, which is so-called the rescaling refractive index *(n')*, is obtained as

$$n'(x, y) = \left|\nabla S(u)\right| = \left|\frac{dS}{du}\right| n(x, y) \tag{7}$$

Furthermore, the refractive index changes, but the rays shape and the phase-front have not. Thus, there is no disruption in the performance of the structure. As a result, we can change the refractive index to values greater than one in physical space by selecting a suitable increasing function. Hence, we choose one of the two rays with the lowest refractive index value according to Fig. 4. Since this ray does not include the whole optical path length, we must consider another suitable increasing function for the rest. Therefore, we divide the optical path into two parts, from $u_0$ to $u_1$ (0 to 25mm) and $u_1$ to $u_2$ (25mm to 75mm). The reflector body in virtual space (Fig. 3a) is free space (i.e., n=1), so according to Eq. 5, the optical path length is equal to the structure width (or $v$ coordinate). For the first part, $u_0$ to $u_1$, we define $S(u)$ as a polynomial series of degree three. This function should be continuous at $u_1$, and $u_0$ is selected according to the refractive index at this point. We apply genetic algorithm optimization to obtain polynomial coefficients by considering the constraints.

For $u_1$ to $u_2$ an increasing function is applied along the selected ray in Fig.4 as

$$S(u) = \int_{u_1}^{u_2} \frac{1}{n(u)} du \tag{8}$$

Where $n(u)$ is the refractive index versus the optical path along the desired ray, and integration is also applied to this ray from $u_1$ to $u_2$.

Figure. 5 presents the increasing function $S(u)$ and its first derivative $dS/du$. The rescaling refractive index is shown in Fig. 6. It can be seen that there is no sub-unit value, and the refractive index values are increased to one ($n$=1) in the left and right of the reflector. The continuous refractive index profile is divided into several regions with almost the same refractive index for the practical realization of the antenna. These contours are shown in Fig.6 as well.

We can remove the sections corresponding to regions 1, 2, and 3 in Figure 6, which most of these areas have a refractive index of 1, 1.03, and 1.1, respectively. These regions do not affect the structure performance due to the distance from the reflector PEC section. Therefore, we put aside the regions whose refractive index values are nearly one, as shown in Fig. 7.

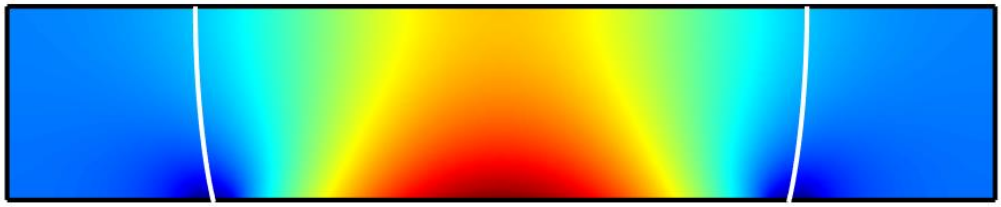

**Figure 4.** The selected ray to apply the rescaling refractive index method.

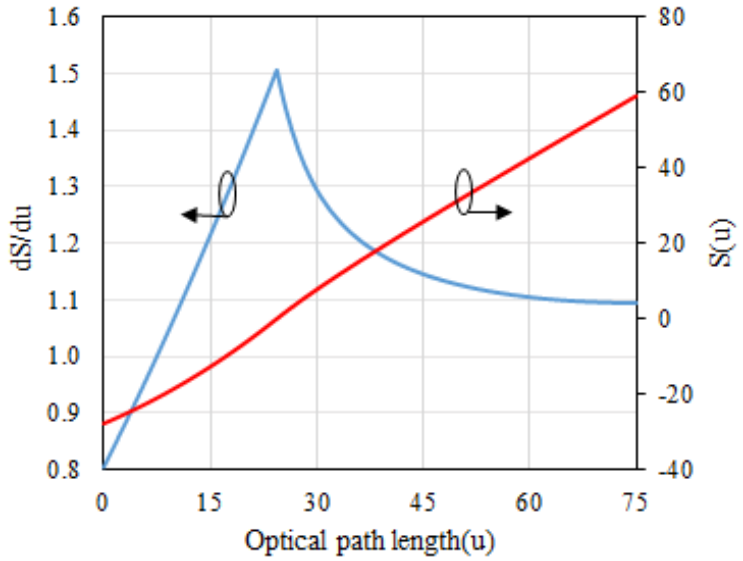


**Figure 5.** The increasing function *S(u)* and its first derivative *dS/du*.

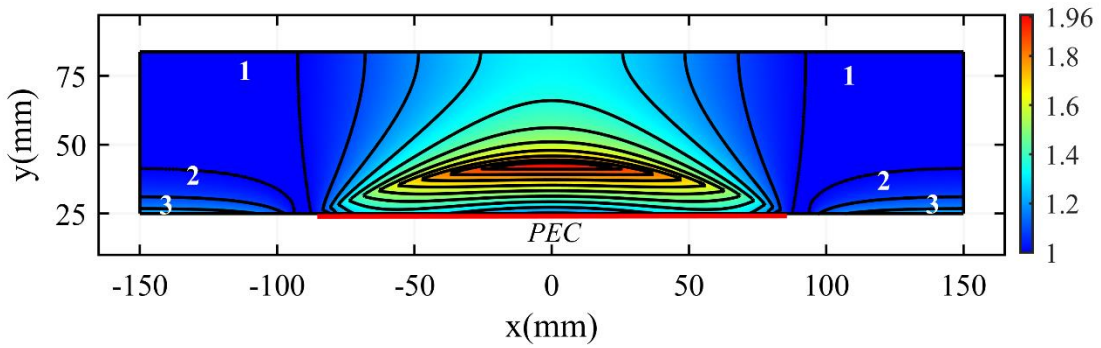


**Figure 6.** The flat reflector antenna's rescaling refractive index. The borders of regions with almost the same refractive index are shown by the sketched outlines with black lines.

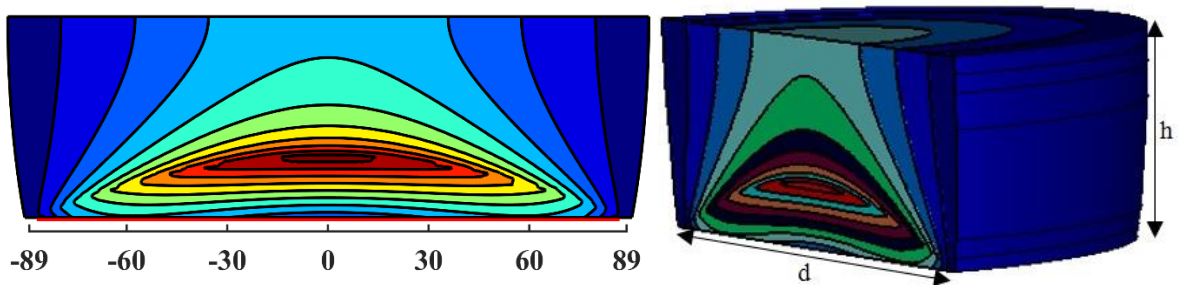


**Figure 7.** Final profile of the reflector antenna. (a) two-dimensional, (b) 3-dimensional cross-section (h=58.7mm, d=178mm).

## Simulation Results

In this section, we present the simulation results by COMSOL Multiphysics. Eleven layers make up the proposed antenna, with permeability coefficients ranging from 1.1 to 3.8. The number of layers is determined by the precision of the antenna's focus point, resulting in a focal length of 100mm (as the equivalent parabolic antenna). Rotating the permeability profile around the propagation direction yields the final three-dimensional profile of the flat reflector antenna. To do this, we used 2-D Axisymmetric in COMSOL Multiphysics that rotates the simulated 2D environment around the vertical axis. Two-dimensional and three-dimensional structure of the flat reflector is shown in Fig.7. The height and diameter of the antenna are 58.7*mm* and 178*mm*, respectively.

At first, a plane wave is sent to the two-dimensional structure of the antenna. Figure. 8a presents the simulated electric field magnitude of the antenna at 15 GHz. It can be seen that the incident plane wave is concentrated at a point on the antenna axis with $y$=100*mm*, which is better shown in Fig. 8b, showing the electric field along the focal length.

In the next simulation, a feeding horn antenna is located in the focal point to verify the radiation properties of the flat antenna. Fig. 9a shows the flat antenna and its feed in the COMSOL Multiphysics. The feed antenna is a conical horn connected to a standard KU-band circular waveguide with a diameter of $a$=15.08 *mm*, and length of $L_1$=4*mm*. Moreover, the diameter and length of the horn are $b$=19 *mm* and $L_2$=6 *mm* respectively, as shown in Fig. 9b. Furthermore, we simulate the antenna in CST Studio Suite software to confirm the simulation results. Fig. 9c indicates the simulated antenna in CST.

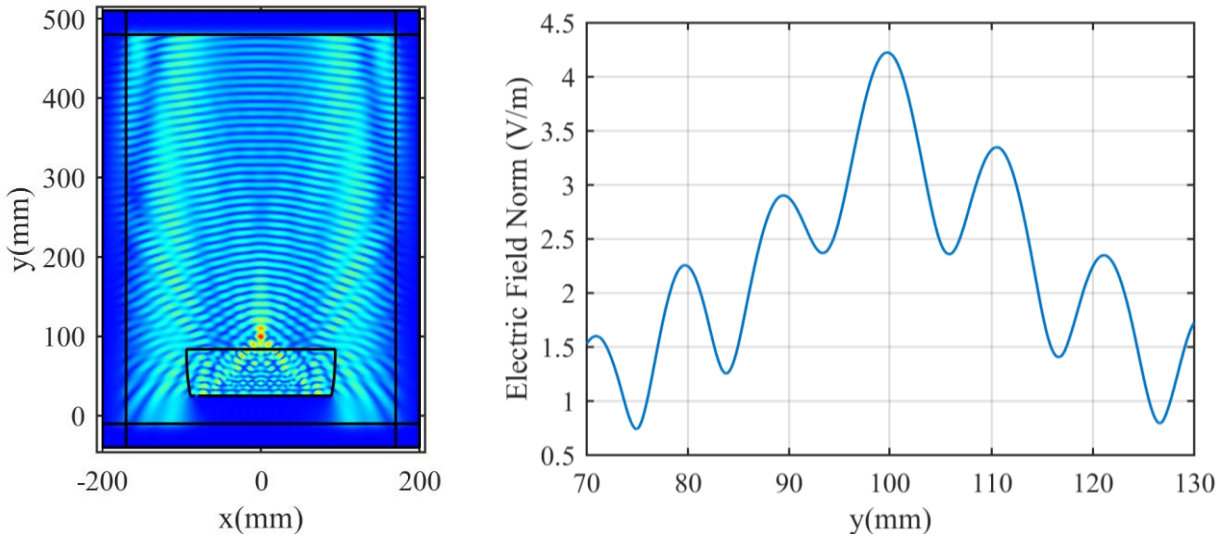


(a) (b)

**Figure 8.** Electric field magnitude of the antenna, (a) 2-dimensional structure, and (b) along the focal length.

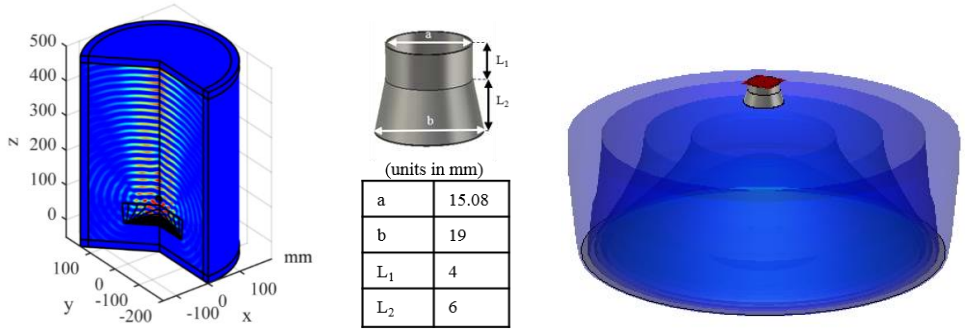


(units in mm)

| | |
|---|---|
| a | 15.08 |
| b | 19 |
| $L_1$ | 4 |
| $L_2$ | 6 |

(a) (b) (c)

**Figure 9.** 3D structure of the flat reflector with feeding horn antenna, (a) the simulated antenna in COMSOL, (b) feeding horn antenna with specified dimensions in mm, (c) simulated antenna in CST.

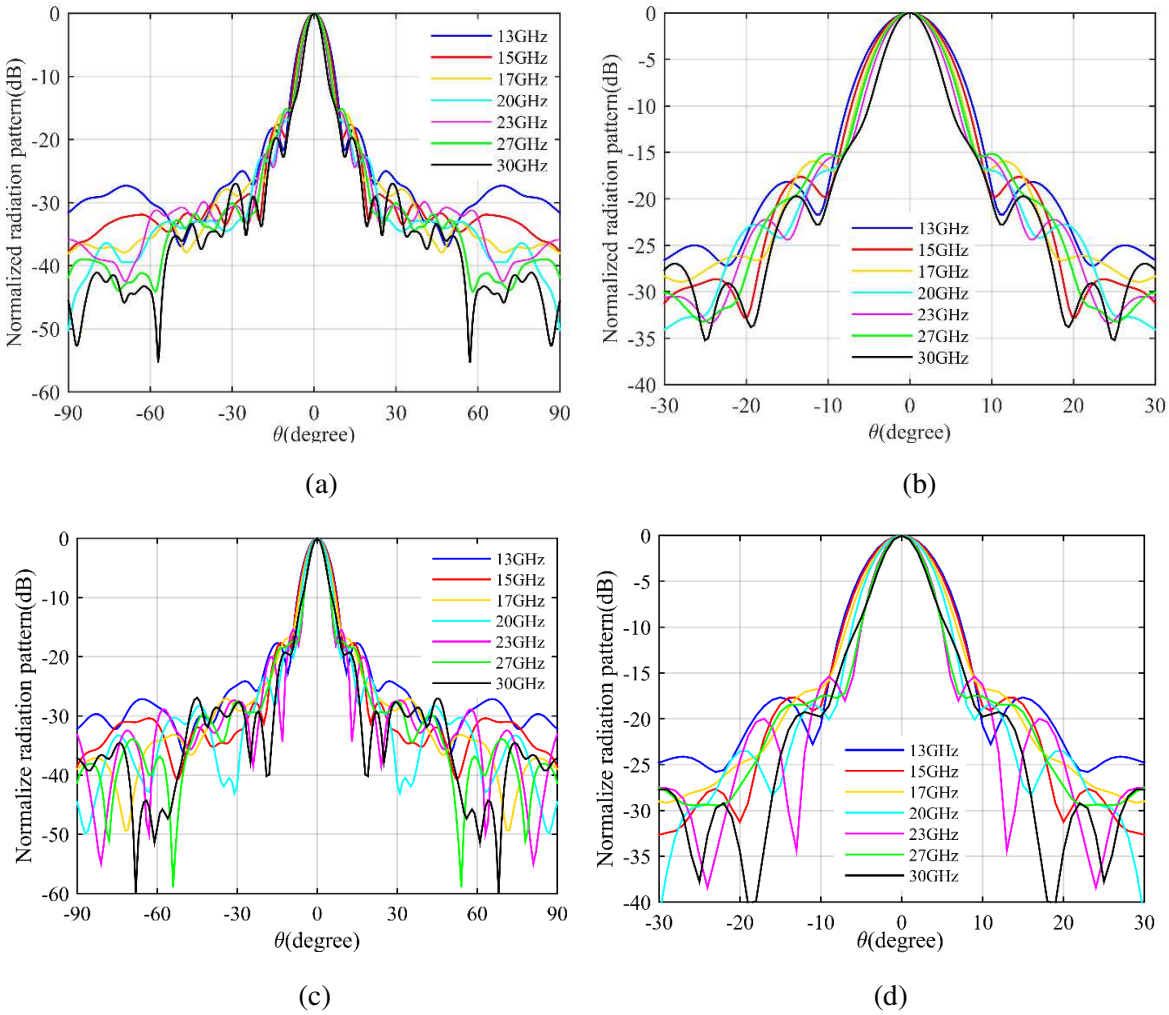


(a) (b) (c) (d)

**Figure 10.** Simulated normalized radiation pattern of the antenna in the H-plane, (a) using COMSOL, (b) the corresponding magnified picture, (c) using CST, and (d) the corresponding magnified picture.

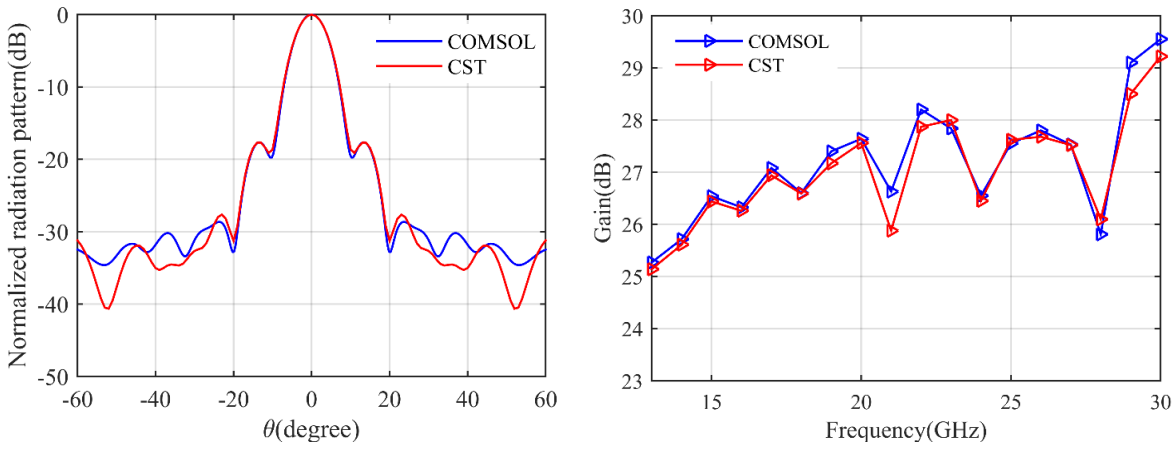


(a) (b)

**Figure 11.** Comparing COMSOL and CST simulation results, (a) radiation pattern at 15 GHz, (b) gain of the antenna.

The simulated normalized radiation pattern of the antenna using COMSOL is shown in Fig. 10a and Fig. 10b at various frequencies in the range from 13-30 GHz. Fig. 10c and Fig. 10d show the corresponding results using CST which shows the half-power beamwidth (HPBW) decreases from 8.6° to 5.1°, when the frequency increases from 13 to 30 GHz . The side-lobe levels are below -15dB at all frequencies, indicating the proper performance of the antenna. The radiation pattern results of COMSOL and CST are compared at f=15 GHz in Fig.11a which shows the CST results matches very well with the COMSOL results. Figure.11b presents the antenna gain which shows a proper gain and a good match among the results of two simulation software. Eventually, the proposed flat reflector antenna can be realized using eleven milled dielectric layers with different permittivity[38].

## Conclusion

We introduced an implementable broadband flat reflector based on conformal transformation optics. The proposed antenna needs only dielectric materials with permittivity greater than one which is divided into eleven layers with permittivity of 1.1 to 3.8, making it a realizable and ultra-wideband flat reflector in the frequency range from 13 to 30 GHz. The simulated antenna gain is about 25.27 to 29.55 dB, with the side-lobe level below -15 dB. Moreover, the half-power beamwidth varies from 8.6° to 5.1° in the frequency range from 13 to 30 GHz. The simulation results are verified with COMSOL Multiphysics and CST Studio Suite software.

## References

1. Pendry, J. B., Schurig, D. & Smith, D. R. Controlling electromagnetic fields. *Sci* **312**, 1780–1782, http://doi.org/10.1126/science.1125907 (2006).
2. Werner, D. H. Transformation Electromagnetics and Metamaterials. *Springer,* http://doi.org/10.1007/978-1-4471-4996-5 (2014).
3. Ruan, Z., Yan, M., Neff, C. W. & Qiu, M. Ideal cylindrical cloak: Perfect but sensitive to tiny perturbations. *Phys. Rev. Lett.* **99**, 1–4, https://doi.org/10.1103/PhysRevLett.99.113903 (2007).
4. Keivaan, A., Fakheri, M. H., Abdolali, A., Member, S. & Oraizi, H. Design of Coating Materials for Cloaking and Directivity Enhancement of Wire Antennas Using Transformation Optics. *IEEE*

*Antennas Wirel. Propag. Lett.* **16**, http://doi.org/10.1109/LAWP.2017.2764064 (2017).
5. Liu, R . Ji, C. Mock, J,J . Chin, J, Y. Broadband Ground-Plane Cloak. *Sci* **323**, 366–369, http://doi.org/ 10.1126/science.1166949 (2009).
6. Yang, Y., Chen, H., Yu, F., Li, E. & Chen, H. A full-parameter, broadband, homogeneous, and compact waveguide coupler designed with transformation optics. *IEEE Antennas Wirel. Propag. Lett.* **14**, 634–637, http://doi.org/ 10.1109/LAWP.2014.2376179 (2014).
7. Eskandari, H., Attari, A. R. & Majedi, M. S. Reflectionless design of a nonmagnetic homogeneous optical waveguide coupler based on transformation optics. *J. Opt. Soc. Am. B* **35**, 54–60, https://doi.org/10.1364/JOSAB.35.000054 (2018).
8. Kwon, D. & Member, S. Quasi-Conformal Transformation Optics Lenses for Conformal Arrays. *IEEE Antennas Wirel. Propag. Lett.* **11**, 1125–1128, http://doi.org/ 10.1109/LAWP.2012.2218092 (2012).
9. Ebrahimpouri, M., Member, S. & Quevedo-teruel, O. Bespoke Lenses Based on Quasi Conformal Transformation Optics Technique. *IEEE Antennas Wirel. Propag. Lett.* **65**, 2256–2264, http://doi.org/ 10.1109/TAP.2017.2679494 (2017).
10. Luo, Y., Zhang, J., Ran, L., Chen, H. & Kong, J. A. New concept conformal antennas utilizing metamaterial and transformation optics. *IEEE Antennas Wirel. Propag. Lett.* **7**, 509–512, http://doi.org/ 10.1109/LAWP.2008.2002537 (2008).
11. Tichit, P. H., Burokur, S. N. & Lustrac, A. De. Ultra directive antenna via transformation optics. *J. Appl. Phys.* **105**, 3–5, https://doi.org/10.1063/1.3131843 (2009).
12. Aghanejad, I., Abiri, H. & Yahaghi, A. Design of high-gain lens antenna by gradient-index metamaterials using transformation optics. *IEEE Transaction on Antennas Propag.* **60**, 4074–4081, http://doi.org/ 10.1109/TAP.2012.2207051 (2012).
13. Amarasinghe, Y., Mendis, R., Shrestha, R., Guerboukha, H. & Taiber, J. Broadband wide - angle terahertz antenna based on the application of transformation optics to a Luneburg lens. *Sci. Rep.* **11**, 1–8, https://doi.org/10.1038/s41598-021-84849-8 (2021).
14. Eskandari, H., Saviz, S. & Tyc, T. Directivity enhancement of a cylindrical wire antenna by a graded index dielectric shell designed using strictly conformal transformation optics. *Sci. Rep.* **11**, 1–11, https://doi.org/10.1038/s41598-021-92200-4 (2021).
15. Eskandari, H., Albadalejo-Lijarcio, J. L., Zetterstrom, O., Tyc, T. & Quevedo-Teruel, O. H-plane horn antenna with enhanced directivity using conformal transformation optics. *Sci. Rep.* **11**, 1–9, https://doi.org/10.1038/s41598-021-93812-6 (2021).
16. Nazarzadeh, F. & Heidari, A. . Design of a New Cylindrical to Plane Wave Transformer Based on Transformation Optics. *28th Iran. Conf. Electr. Eng.* 1–4, http://doi.org/ 10.1109/ICEE50131.2020.9260913 (2020).
17. Zhou, J., Li, M., Xie, L. & Liu, D. Design of a new kind of polarization splitter based on transformation optics. *Optik* **122**, 1672–1675, https://doi.org/10.1016/j.ijleo.2010.10.023 (2011).
18. Mousavi, S. S. S., Majedi, M. S. & Eskandari, H. Design and simulation of polarization transformers using transformation electromagnetics. *Optik* **130**, 1099–1106, https://doi.org/10.1016/j.ijleo.2016.11.129 (2017).
19. Zhai, T., Zhou, Y., Zhou, J. & Liu, D. Polarization controller based on embedded optical transformation. *Opt. Express* **17**, 17206–17213, https://doi.org/10.1364/OE.17.017206 (2009).
20. Kwon, D.-H. & Werner, D. H. Polarization splitter and polarization rotator designs based on transformation optics. *Opt. Express* **16**, 18731–18738, https://doi.org/10.1364/OE.16.018731 (2008).
21. Rahm, M., Roberts, D. A., Pendry, J. B. & Smith, D. R. Transformation-optical design of adaptive beam bends and beam expanders. *Opt. Express* **16**, 11555–11567, https://doi.org/10.1364/OE.16.011555 (2008).
22. Jiang, W. X., Cui, T. J., Zhou, X. Y., Yang, X. M. & Cheng, Q. Arbitrary bending of electromagnetic waves using realizable inhomogeneous and anisotropic materials. *Phys. Rev. E* **78**, 1–4, https://doi.org/10.1103/PhysRevE.78.066607 (2008).

23. Pakniyat, S., Jam, S., Yahaghi, A. & Hanson, G. W. Reflectionless plasmonic right-angled waveguide bend and divider using graphene and transformation optics. *Opt. Express* **29**, 9589–9598, https://doi.org/10.1364/OE.417678 (2021).
24. Leonhardt, U. Optical conformal mapping. *Sci* **312**, 1777–1780, http://doi.org/10.1126/science.1126493 (2006).
25. Xu, L. & Chen, H. Conformal transformation optics. *Nat. Photonics* **9**, 15–23, http://doi.org/10.1038/nphoton.2014.307 (2015).
26. Chang, Z., Zhou, X., Hu, J. & Hu, G. Design method for quasi-isotropic transformation materials based on inverse Laplace ' s equation with sliding boundaries. *Opt. Express* **18**, 6089–6096, https://doi.org/10.1364/OE.18.006089 (2010).
27. Li, S., Zhang, Z., Wang, J. & He, X. Design of conformal lens by drilling holes materials using quasi-conformal transformation optics. *Opt. Express* **22**, 25455–25465, https://doi.org/10.1364/OE.22.025455 (2014).
28. Gabrielli, L. H. & Lipson, M. Transformation optics on a silicon platform. *journals Opt.* **13**, https://doi.org/10.1088/2040-8978/13/2/024010 (2010).
29. Falco, A. Di, Kehr, S. C. & Leonhardt, U. Luneburg lens in silicon photonics. *Opt. Express* **19**, 5156–5162, https://doi.org/10.1364/OE.19.005156 (2011).
30. Gilarlue, M. M., Badri, S. H., Saghai, H. R., Nourinia, J. & Ghobadi, C. Photonic crystal waveguide intersection design based on Maxwell ' s fish- eye lens. *Photonics Nanostructures-Fundamentals Appl.* **31**, 154–159, https://doi.org/10.1016/j.photonics.2018.08.001 (2018).
31. Tang, W., Argyropoulos, C., Kallos, E., Song, W. & Hao, Y. Discrete coordinate transformation for designing all-dielectric flat antennas. *IEEE Transaction on Antennas Propag.* **58**, 3795–3804, http://doi.org/ 10.1109/TAP.2010.2078475 (2010).
32. Yang, R., Tang, W. & Hao, Y. Wideband beam-steerable flat reflectors via transformation optics. *IEEE Antennas Wirel. Propag. Lett.* **10**, 1290–1294, http://doi.org/ 10.1109/LAWP.2011.2176461 (2011).
33. Eskandari, H. & Tyc, T. Controlling refractive index of transformation-optics devices via optical path rescaling. *Sci. Rep.* **9**, 1–12, https://doi.org/10.1038/s41598-019-54516-0 (2019).
34. Heidari, A., Ghafoorzadeh-Yazdi, A. & Bakhoda, M. Wideband reflectarray antenna using logarithmic patch element. *Int J of RF Microw C E.* **30**, http://doi.org/10.1002/mmce.22377 (2020).
35. Liang, L. & Hum, S. V. Wide-angle scannable reflector design using conformal transformation optics. *Opt. Express.* **21**, 2133–2146, https://doi.org/10.1364/OE.21.002133 (2013).
36. Turpin, J. P., Massoud, A. T., Jiang, Z. H., Werner, P. L. & Werner, H. Conformal mappings to achieve simple material parameters for transformation optics devices. *Opt. Express* **18**, 244–252, https://doi.org/10.1364/OE.18.000244 (2010).
37. Burokur, S, N. Transformation Optics-based Antennas. *Elsevier*, http://doi.org/10.1016/C2016-0-00816-1 (2016).
38. Ebrahimpouri, M., Zetterstrom, O. & Quevedo-Teruel, O. Experimental Validation of a Bespoke Lens for a Slot Log-Spiral Feed. *IEEE Antennas Wirel. Propag. Lett.* **19**, 557–560, http://doi.org/ 10.1109/LAWP.2020.2971852 (2020).